HHS Public Access

Author manuscript

Oncogene. Author manuscript; available in PMC 2012 September 01.

Published in final edited form as:

Oncogene. 2012 March 1; 31(9): 1155–1165. doi:10.1038/onc.2011.303.

Absence of Wip1 partially rescues Atm deficiency phenotypes in mice

Yolanda Darlington[1,2], **Thuy-Ai Nguyen**[1,2], **Sung-Hwan Moon**[2,3], **Alan Herron**[4], **Pulivarthi Rao**[5], **Chengming Zhu**[6], **Xiongbin Lu**[7], and **Lawrence A. Donehower**[1,2,3,5]

[1]Interdepartmental Graduate Program in Cell and Molecular Biology

[2]Department of Molecular Virology and Microbiology, Baylor College of Medicine, Houston, Texas 77030

[3]Department of Molecular and Cellular Biology, Baylor College of Medicine, Houston, Texas 77030

[4]Department of Pathology and Immunology and Center for Comparative Medicine, Baylor College of Medicine, Houston, Texas 77030

[5]Department of Pediatrics, Baylor College of Medicine, Houston, Texas 77030

[6]Departments of Immunology, The University of Texas M.D. Anderson Cancer Center, Houston, TX 77030

[7]Department of Cancer Biology, The University of Texas M.D. Anderson Cancer Center, Houston, TX 77030

Abstract

Wildtype p53-Induced Phosphatase 1 (WIP1) is a serine/threonine phosphatase that dephosphorylates proteins in the ataxia telangiectasia mutated (ATM)-initiated DNA damage response pathway. WIP1 may play a homeostatic role in ATM signaling by returning the cell to a normal pre-stress state following completion of DNA repair. To better understand the effects of WIP1 on ATM signaling, we crossed *Atm*-deficient mice to *Wip1*-deficient mice and characterized phenotypes of the double knockout progeny. We hypothesized that the absence of Wip1 might rescue Atm deficiency phenotypes. *Atm* null mice, like *ATM*-deficient humans with the inherited syndrome ataxia telangiectasia, exhibit radiation sensitivity, fertility defects, and are T-cell lymphoma prone. Most double knockout mice were largely protected from lymphoma development and had a greatly extended lifespan compared to *Atm* null mice. Double knockout mice had increased p53 and H2AX phosphorylation and p21 expression compared to their *Atm* null counterparts, indicating enhanced p53 and DNA damage responses. Additionally, double knockout splenocytes displayed reduced chromosomal instability compared to *Atm* null mice.

Correspondence to: Lawrence A. Donehower, Department of Molecular Virology and Microbiology, Baylor College of Medicine, One Baylor Plaza, Houston, Texas 77030 USA, Phone: 713-798-3594, FAX: 713-798-3490, larryd@bcm.tmc.edu.

Conflict of Interest

There are no competing financial interests in relation to the work described for any of the authors.

Finally, doubly null mice were partially rescued from infertility defects observed in *Atm* null mice. These results indicate that inhibition of WIP1 may represent a useful strategy for cancer treatment in general and A-T patients in particular.

Keywords

WIP1; PPM1D; ATM; ataxia telangiectasia; p53; thymic lymphoma

Introduction

The capacity of cells to recognize and repair DNA damage is crucial for maintaining genomic stability and preventing cancer. The importance of DNA damage response mechanisms is made obvious when one of its key components is rendered defective in human genetic disorders such as ataxia-telangiectasia (A-T). A-T is a rare autosomal recessive syndrome characterized by progressive neurodegeneration, radiosensitivity, immune dysfunction, cell-cycle checkpoint defects, genomic instability, and an increased predisposition to cancer (Chun and Gatti, 2004). Shiloh and co-workers first cloned the defective gene responsible for A-T, the *ataxia telangiectasia mutated (ATM)* gene (Savitsky *et al.*, 1995). Most mutations in the *ATM* gene result in an absence of a full-length, functional protein product (Chun and Gatti, 2004).

ATM is one of six members of the phosphoinositide 3-kinase-related protein kinase (PIKK) family that include other DNA damage response sensors such as ATM and Rad3-related protein (ATR) and DNA dependent protein kinase catalytic subunit (DNA-PKcs). The *ATM* gene encodes a serine/threonine kinase that is a critical DNA damage sensor that activates cell cycle control and DNA repair pathways (Shiloh, 2003; Lavin, 2008; Abraham, 2001). ATM phosphorylates and activates numerous target proteins involved in initiation and maintenance of cell cycle checkpoints such as CHK2, p53, MDM2, SMC1, and CDC25C (Shiloh, 2003). The phosphorylation of p53 at serine 15 and at serine 20 via activation of CHK2 are important components of ATM signaling, as p53 is a critical modulator of both the G1 and G2/M checkpoints (Appella and Anderson, 2001).

One important tool aiding our understanding of ATM functions has been the development of *Atm* null mice, which recapitulate many of the phenotypes that are observed in A-T patients (Xu *et al.*, 1996; Barlow *et al.*, 1996; Elson *et al.*, 1996; Herzog *et al.*, 1998). Like A-T patients, *Atm* null mice are prone to developing T-cell lymphomas. $Atm^{-/-}$ mice usually die between 3-6 months of age (Xu *et al.*, 1996; Barlow *et al.*, 1996; Elson *et al.*, 1996). Additionally, *Atm* null mice are hypersensitive to radiation, are infertile, have immune system abnormalities, motor coordination defects, and a reduced body size (Barlow *et al.*, 1996; Xu *et al.*, 1996; Rotman and Shiloh, 1998; Westphal *et al.*, 1997; Elson *et al.*, 1996; Herzog *et al.*, 1998).

The ATM-initiated kinase cascade activates cell cycle checkpoints and DNA repair pathways. But once the damage is repaired, how is the cell returned to a pre-stress state? Phosphatases are obvious candidates as homeostatic regulators of ATM-initiated phosphorylations. One such candidate is the Wild-type p53-induced phosphatase 1 (WIP1),

a type 2C serine/threonine phosphatase that is induced in response to DNA damage in a p53-dependent manner (Fiscella *et al.*, 1997). WIP1 dephosphorylates multiple proteins in the ATM/ATR DNA damage response pathway, such as CHK1, CHK2, p53, MDM2, and H2AX (Takekawa *et al.*, 2000; Lu *et al.*, 2005a; Lu *et al.*, 2007; Fujimoto *et al.*, 2006; Shreeram *et al.*, 2006a; Macurek *et al.*, 2010; Moon *et al.*, 2010). WIP1 dephosphorylates the same sites (pS/pTQ motifs) that are phosphorylated by ATM and ATR. Moreover, WIP1 dephosphorylates ATM itself and suppresses its activity (Shreeram *et al.*, 2006a). Importantly, WIP1 suppresses p53 by multiple mechanisms, including dephosphorylation of p53 kinases (ATM, CHK1, CHK2) (Lu *et al.*, 2005b; Shreeram *et al.*, 2006b; Fujimoto *et al.*, 2006), p53 itself (at serine 15) (Lu *et al.*, 2005b), and MDM2, which facilitates MDM2-mediated degradation of p53 (Lu *et al.*, 2008). We hypothesize that WIP1 facilitates reversal of the ATM/ATR-initiated kinase cascade and reverts the cell to a pre-stress state following completion of DNA repair (Lu *et al.*, 2008).

WIP1 has been shown to be an oncogene and is amplified and overexpressed in several human tumor types (Bulavin *et al.*, 2002; Li *et al.*, 2002; Hirasawa *et al.*, 2003; Saito-Ohara *et al.*, 2003; Ehrbrecht *et al.*, 2006; Castellino *et al.*, 2008; Loukopoulos *et al.*, 2007). On the other hand, mice lacking Wip1 are resistant to spontaneous and oncogene-induced tumors, most likely due to enhanced DNA damage and p53 responses (Nannenga *et al.*, 2006; Choi *et al.*, 2002; Bulavin *et al.*, 2004; Harrison *et al.*, 2004; Shreeram *et al.*, 2006b). WIP1 inhibitors have been shown to reduce tumor cell proliferation, suggesting that inhibition of WIP1 may be a beneficial cancer therapeutic tool (Belova *et al.*, 2005; Rayter *et al.*, 2008; Tan *et al.*, 2009; Yamaguchi *et al.*, 2006; Saito-Ohara *et al.*, 2003; Yoda *et al.*, 2008).

Because of the relationship between ATM/ATR phosphorylation and WIP1 dephosphorylation targets, we hypothesized that ATM deficiency phenotypes resulting from inefficient phosphorylation of normal ATM targets might be rescued by eliminating WIP1 function. Presumably, in ATM deficiency there is some phosphorylation of ATM targets by related PIKKs such as ATR and DNA-PKcs, but this compensatory phosphorylation is inadequate to prevent the ATM deficiency phenotypes. However, the absence of WIP1 might enhance or prolong phosphorylation of some ATM target proteins and rescue some of the ATM deficiency phenotypes. We tested this hypothesis by crossing *Atm*-deficient mice to *Wip1*-deficient mice to obtain $Atm^{-/-}Wip1^{-/-}$ double knockout mice. Here, we show that the absence of Wip1 in an *Atm* null background partially rescues some Atm deficiency phenotypes. Compared to $Atm^{-/-}$ mice, $Atm^{-/-}Wip1^{-/-}$ mice displayed reduced tumorigenesis and dramatically enhanced longevity, as well as partial rescue of chromosomal instability and gametogenesis. Thus, inhibition of WIP1 may represent a viable approach for treating cancer and some phenotypes associated with ATM deficiency.

Results

Absence of Wip1 largely rescues lymphomagenesis in Atm null mice

Atm null mice succumb to thymic lymphomas at 3-6 months of age (Barlow *et al.*, 1996; Elson *et al.*, 1996; Xu *et al.*, 1996; Westphal *et al.*, 1997). Because WIP1 dephosphorylates some of the same targets that ATM phosphorylates, we hypothesized that the absence of Wip1 might rescue some of the deleterious phenotypes in the *Atm* null mice. To test this

hypothesis, $Atm^{+/-}Wip1^{+/+}$ mice were crossed to $Atm^{+/+}Wip1^{+/-}$ mice, and double heterozygous F1 progeny were re-crossed to obtain F2 $Atm^{+/+}Wip1^{+/+}$, $Atm^{-/-}Wip1^{+/+}$, $Atm^{-/-}Wip1^{+/-}$, and $Atm^{-/-}Wip1^{-/-}$ mice. A minimum of 43 mice for each genotype were monitored over their entire lifespan. As expected, $Atm^{+/+}Wip1^{+/+}$ mice live relatively normal lifespans of over two years (Fig. 1A). Consistent with previous reports, 95% of $Atm^{-/-}Wip1^{+/+}$ mice developed thymic lymphomas by 150 days of age, and all are dead by 300 days of age (Fig. 1A). Conversely, only 11% of $Atm^{-/-}Wip1^{-/-}$ mice develop thymic lymphomas by 150 days of age, and rarely developed tumors after 180 days (6 months). The majority of the double knockout mice exhibited dramatically enhanced longevities compared to *Atm* null mice, with median lifespans of 620 and 110 days, respectively (Fig. 1A). No Wip1 dosage effect was observed, as $Atm^{-/-}Wip1^{+/-}$ mice developed tumors at the same rate as $Atm^{-/-}Wip1^{+/+}$ mice. Thus, the absence of Wip1 largely rescues tumor susceptibility phenotypes observed in *Atm* null mice.

To determine if there were any differences among the tumors that developed in the $Atm^{-/-}Wip1^{+/+}$, $Atm^{-/-}Wip1^{+/-}$, and $Atm^{-/-}Wip1^{-/-}$ mice, tumors were collected from the mice. Gross necropsies revealed only thymic tumors in $Atm^{-/-}Wip1^{+/+}$, $Atm^{-/-}Wip1^{+/-}$, and $Atm^{-/-}Wip1^{-/-}$ mice. Analysis of hematoxylin and eosin (H&E) stained tumor sections confirmed that all tumors were thymic lymphomas of likely T-cell origin, and no histopathological differences were observed among the $Atm^{-/-}Wip1^{+/-}$, $Atm^{-/-}Wip1^{-/-}$ and $Atm^{-/-}Wip1^{+/+}$ lymphomas (Fig. 1B-D).

$Atm^{-/-}Wip1^{-/-}$ mice exhibit enhanced p53 and DNA damage responses

The reduced tumor incidence in the $Atm^{-/-}Wip1^{-/-}$ mice compared to *Atm* null mice is consistent with enhanced DNA damage and p53 responses. To examine this further, $Atm^{+/+}Wip1^{+/+}$, $Atm^{+/+}Wip1^{-/-}$, $Atm^{-/-}Wip1^{+/+}$, and $Atm^{-/-}Wip1^{-/-}$ eight week old mice were irradiated with 5 Gy of ionizing radiation (IR). Thymi were harvested six hours after IR and analyzed for phosphorylation status of known Wip1 dephosphorylation targets. Lysates from normal thymi and spleens were assessed by Western blot analysis with antibodies to p53 and H2AX as well as phospho-specific antibodies for p53 (pS18) and γ H2AX (pS140). Both of these phosphorylation events are markers for an activated DNA damage response. Basal levels of γ-H2AX and phospho-p53 were low in unirradiated $Atm^{+/+}Wip1^{+/+}$ lymphoid tissues but were induced to moderate levels six hours after IR treatment (Fig. 2A; Fig. S1). Irradiated $Atm^{+/+}Wip1^{-/-}$ thymi and spleens exhibited increased phosphorylation of H2AX and p53 compared to irradiated $Atm^{+/+}Wip1^{+/+}$ thymi and spleens. Surprisingly, deletion of *Atm* did not impair IR-induced phosphorylation of H2AX and p53 and was comparable to $Atm^{+/+}Wip1^{+/+}$ levels (Fig. 2A-C). This is likely a result of compensatory phosphorylation by other PIKKs. In the presence of IR damage, the $Atm^{-/-}Wip1^{-/-}$ thymi exhibited high phosphorylation levels of H2AX and p53 comparable to $Atm^{+/+}Wip1^{-/-}$ thymi (Fig. 2A-C). In addition, IR treatment resulted in increased p53 protein levels across all four genotypes, as expected. Absence of *Wip1* in $Atm^{+/+}$ and $Atm^{-/-}$ mice conferred modestly increased p53 protein stability after IR compared to wildtype and *Atm* null mice (Fig. 2A). Finally, irradiation of the different Atm/Wip1 genotype mice resulted in similar patterns of enhanced phosphorylation of Brca1 Ser1423 in the absence of

Wip1 (Fig. S2). This Brca1 phosphorylation site, targeted by Atm, is also dephosphorylated by Wip1 (Nguyen and Donehower, unpublished data).

The increased p53 protein levels in irradiated $Atm^{+/+}Wip1^{-/-}$ and $Atm^{-/-}Wip1^{-/-}$ thymi and spleens suggested a corresponding increase in p53 activity. To test this, we measured $p21^{Waf1/Cip1}$ RNA expression levels in unirradiated and irradiated thymi of all four genotypes by real-time quantitative RT-PCR. The p21 gene is a direct transcriptional target of activated p53 and is a prototypical marker for p53 functional activity (El-Deiry *et al.*, 1993). IR results in a roughly 20-fold increase in p21 RNA expression in $Atm^{+/+}Wip1^{+/+}$ thymi and this is further increased to a 30-fold induction in $Atm^{+/+}Wip1^{-/-}$ thymocytes (Fig. 2D). Importantly, IR-induced p21 RNA is only induced about 7-fold in $Atm^{-/-}Wip1^{+/+}$ thymocytes, indicating loss of p53 activity in the absence of Atm. However, this p53 activity loss is partially rescued in double knockout thymi, which exhibit a 16-fold IR-induction of p21 RNA (Fig. 2D). Overall, these results indicate that the absence of Wip1 results in enhanced p53 and DNA damage responses in both $Atm^{+/+}Wip1^{-/-}$ and $Atm^{-/-}Wip1^{-/-}$ tissues.

Absence of Wip1 reduces chromosomal instability in Atm null splenocytes

Previously, spectral karyotyping (SKY) analysis revealed that both murine *Atm* null fibroblasts and A-T cells from humans display increased chromosomal instability (Barlow *et al.*, 1996; Chun and Gatti, 2004). Since the $Atm^{-/-}Wip1^{-/-}$ mice have enhanced DNA damage responses, we hypothesized that cells from these mice might also have reduced chromosomal instability. To test this, splenocytes from $Atm^{+/+}Wip1^{+/+}$, $Atm^{+/+}Wip1^{-/-}$, $Atm^{-/-}Wip1^{+/+}$, and $Atm^{-/-}Wip1^{-/-}$ eight week old mice were isolated, mitogen-activated, and subjected to SKY analysis. No aberrations were detected in metaphase chromosomes from 12-20 metaphase profiles prepared from each of four $Atm^{+/+}Wip1^{+/+}$ and four $Atm^{+/+}Wip1^{-/-}$ mice (Fig. 3A,B). SKY analysis of splenocyte metaphase spreads from six $Atm^{-/-}Wip1^{+/+}$ mice revealed multiple chromosomal aberrations, including translocations, chromosome losses, and chromosome gains (Fig. 3C,D). Conversely, metaphase spreads from splenocytes of five $Atm^{-/-}Wip1^{-/-}$ mice averaged fewer chromosomal abnormalities than those from $Atm^{-/-}Wip1^{+/+}$ mice (Fig. 3E,F). Overall, *Atm* null splenocytes averaged 18.3 chromosomal aberrations per mouse analyzed, whereas $Atm^{-/-}Wip1^{-/-}$ splenocytes averaged 6.8 chromosomal aberrations per mouse (Fig. 3G). This difference was statistically significant ($P = 0.009$). $Atm^{-/-}Wip1^{+/+}$ mice averaged 1.42 chromosomal aberrations per individual metaphase, while $Atm^{-/-}Wip1^{-/-}$ mice averaged 0.59 chromosomal aberrations per individual metaphase, which was statistically significant ($P = 0.03$) (Fig. 3H). Thus, the absence of Wip1 significantly decreases the genomic instability of *Atm* null cells.

Absence of Wip1 results in partial rescue of gamete formation in Atm null mice

Both A-T patients and *Atm* null mice are infertile (Chun and Gatti, 2004). Testes and ovaries of *Atm* null mice exhibit a disorganized architecture and complete absence of mature gametes (Barlow *et al.*, 1996; Xu *et al.*, 1996; Elson *et al.*, 1996). To test if $Atm^{-/-}Wip1^{-/-}$ mice were rescued from defects in gametogenesis, hematoxylin and eosin staining of tissue sections from testes and ovaries of $Atm^{+/+}Wip1^{+/+}$, $Atm^{+/+}Wip1^{-/-}$, $Atm^{-/-}Wip1^{+/+}$, and $Atm^{-/-}Wip1^{-/-}$ eight week old mice was performed. As expected, testes of $Atm^{+/+}Wip1^{+/+}$

males display a normal seminiferous tubule architecture (Fig. 4A). Testes of the *Atm*$^{+/+}$*Wip1*$^{-/-}$ males revealed reduced numbers of maturing spermatocytes, spermatids, and mature sperm (Fig. 4B), as shown previously (Choi *et al.*, 2002; Nannenga *et al.*, 2006). Testes of *Atm*$^{-/-}$*Wip1*$^{+/+}$ males displayed diffuse hypoplasia of seminiferous tubules with multifocal degeneration of seminiferous tubule epithelium and no spermatogenesis (Fig. 4C). Interestingly, testes from four out of nine *Atm*$^{-/-}$*Wip1*$^{-/-}$ males showed partial restoration of normal seminiferous tubule architecture and maturing spermatocytes, spermatids, and mature sperm similar to those seen in the *Atm*$^{+/+}$*Wip1*$^{-/-}$ testes (Fig. 4D). The other five *Atm*$^{-/-}$*Wip1*$^{-/-}$ males had complete disruption of seminiferous tubule organization and spermatogenesis, evidenced by the absence of spermatids and spermatozoa that was similar to the *Atm* null testes (Fig. 4E).

As expected, ovaries of *Atm*$^{+/+}$*Wip1*$^{+/+}$ females exhibited normal structures (Fig. 4F). Ovaries of *Atm*$^{+/+}$*Wip1*$^{-/-}$ females revealed a reduced number of primordial follicles, oocytes, and developing follicles when compared to *Atm*$^{+/+}$*Wip1*$^{+/+}$ mice (Fig. 4G). Ovaries from *Atm*$^{-/-}$*Wip1*$^{+/+}$ females were devoid of maturing follicles and oocytes (Fig. 4H). However, ovaries from two of four *Atm*$^{-/-}$*Wip1*$^{-/-}$ females displayed formation of primordial follicles, oocytes, and developing follicles similar in number to those seen in the ovaries of the *Wip1* null females (Fig. 4I). Two of the *Atm*$^{-/-}$*Wip1*$^{-/-}$ females had ovaries with no follicles, similar to what is observed in *Atm* null females (Fig. 4J). These results suggest that the absence of Wip1 partially restores gamete formation in *Atm* null mice, but this is an incompletely penetrant phenotype. Moreover, despite apparent partial rescue of gametogenesis in some *Atm*$^{-/-}$*Wip1*$^{-/-}$ animals, these mice never produced offspring in continuous mating with wildtype mice, suggesting that absence of Wip1 was unable to functionally rescue reproductive capacity in *Atm* null mice.

Absence of Wip1 increases IR sensitivity of Atm null mice

Both A-T patients and *Atm* null mice are hypersensitive to IR (Westphal *et al.*, 1997; Barlow *et al.*, 1996; Chun and Gatti, 2004). To test if *Atm*$^{-/-}$*Wip1*$^{-/-}$ mice were rescued from this phenotype, *Atm*$^{+/+}$*Wip1*$^{+/+}$, *Atm*$^{+/+}$*Wip1*$^{-/-}$, *Atm*$^{-/-}$*Wip1*$^{+/+}$, and *Atm*$^{-/-}$*Wip1*$^{-/-}$ six week old mice were subjected to a lethal dose of 8 Gy IR and monitored for survival. *Atm*$^{+/+}$*Wip1*$^{+/+}$ mice died between days 13-30 after IR (Fig. 5A). *Atm*$^{+/+}$*Wip1*$^{-/-}$ mice died between days 11-17 after IR, suggesting a slightly enhanced sensitivity to IR compared to their wildtype counterparts. As anticipated, *Atm*$^{-/-}$*Wip1*$^{+/+}$ mice died more rapidly, between days 4-16. Likewise, *Atm*$^{-/-}$*Wip1*$^{-/-}$ mice died between days 4-10 after IR. Thus, at the 8 Gy dosage, *Atm*$^{-/-}$*Wip1*$^{-/-}$ mice were not rescued from the IR hypersensitivity phenotype of *Atm* null mice. We used a normally sublethal dosage of 4 Gy IR to determine if there were IR sensitivity differences among *Atm*$^{+/+}$*Wip1*$^{+/+}$, *Atm*$^{+/+}$*Wip1*$^{-/-}$, *Atm*$^{-/-}$*Wip1*$^{+/+}$, and *Atm*$^{-/-}$*Wip1*$^{-/-}$ six week old mice. All *Atm*$^{+/+}$*Wip1*$^{+/+}$, *Atm*$^{+/+}$*Wip1*$^{-/-}$, and *Atm*$^{-/-}$*Wip1*$^{+/+}$ mice were monitored for 50 days, and all survived 4 Gy treatment (Fig. 5B). However, 7 of 11 (64%) of the *Atm*$^{-/-}$*Wip1*$^{-/-}$ mice died between days 14 and 30 after 4 Gy IR (Fig. 5B). Thus, rather than rescue IR hypersensitivity, absence of Wip1 further increases the IR sensitivity of *Atm* null mice.

Atm null mice are hypersensitive to IR and die due to severe radiation toxicity of the GI tract (Barlow *et al*., 1996). To determine if GI tracts of the double knockout mice exhibited enhanced radiation toxicity effects, $Atm^{+/+}Wip1^{+/+}$, $Atm^{+/+}Wip1^{-/-}$, $Atm^{-/-}Wip1^{+/+}$, and $Atm^{-/-}Wip1^{-/-}$ six week old mice were subjected to the sub-lethal dose of 4 Gy IR and the small intestines were collected 2, 3, and 4 days after treatment and tissue histopathology was performed. The small intestines of $Atm^{+/+}Wip1^{+/+}$ and $Atm^{+/+}Wip1^{-/-}$ mice appeared largely healthy, whether irradiated or not (Fig. 5C). $Atm^{-/-}Wip1^{+/+}$ mice displayed mild necrosis of the columnar epithelium with an infiltrate of mixed inflammatory cells by the third day post IR. However, small intestines of $Atm^{-/-}Wip1^{-/-}$ mice exhibited a more pronounced radiation toxicity phenotype with moderate to marked loss and shortening of villi with dilatation of glandular crypts accompanied by a slight increase in mitotic figures, and evidence of increased cell death as well as depletion of lymphocytes in the lamina propria (Fig. 5C). Though the small intestines of $Atm^{-/-}Wip1^{-/-}$ mice had a significant radiation toxicity phenotype, it is unclear whether this particular toxicity was responsible for the animals' deaths. We hypothesized that the radiation toxicity phenotype in the $Atm^{-/-}Wip1^{-/-}$ mice may have resulted from enhanced rates of cell apoptosis, but this appears unlikely as thymic tissues from irradiated $Atm^{-/-}Wip1^{-/-}$ mice showed no increase increased in apoptotic markers compared to $Atm^{-/-}Wip1^{+/+}$ or $Atm^{+/+}Wip1^{-/-}$ mice (Fig. S3).

Absence of Wip1 fails to rescue other Atm deficiency phenotypes

Several other Atm deficiency phenotypes were tested for rescue by the absence of Wip1. These included adult body mass (reduced in *Atm* null mice), motor coordination (reduced in *Atm* null mice), lymphocyte numbers (reduced in *Atm* null mice), and T cell maturation (defective in *Atm* null mice). As shown in Figure 6, $Atm^{-/-}Wip1^{-/-}$ mice were comparable to $Atm^{-/-}$ mice in mean body mass at 8 weeks of age (Fig. 6A), length of time maintaining balance on a spinning rota rod (a test of motor coordination) (Fig. 6B), total splenocyte and thymocyte numbers (Fig. 6C), and numbers of CD4+ CD8+ double positive (higher numbers in *Atm* null mice are indicative of defective T cell maturation) and single positive CD4+ thymic T lymphocytes (Fig. 6D). Thus, not all phenotypes associated with Atm deficiency could be rescued or partially rescued by the absence of Wip1.

Discussion

WIP1 dephosphorylates many of the same targets that ATM phosphorylates (Lu *et al*., 2008; Le and Bulavin, 2009). In addition, Shreeram et al. (2006a) have demonstrated that Wip1 directly desphorylates ATM at Ser1981 and is critical for resetting ATM phosphorylation as cells repaired damaged DNA. Because of this antagonistic relationship between ATM and WIP1, we hypothesized that mice lacking Atm, which exhibit many deleterious phenotypes, might benefit from the absence of Wip1. Our hypothesized mechanism for Wip1 rescue was that, despite some compensatory phosphorylation by other PIKKs such as Atr and DNA-PK, many Atm targets would be hypophosphorylated in the absence of Atm. Therefore, the absence of Wip1 would likely increase and prolong the phosphorylation state of hypophosphorylated Atm targets, ultimately restoring a more normal DNA damage response (Fig. 7). If Wip1 absence or inhibition could benefit *Atm* null mice, this could have important implications for A-T patients, as there is currently no effective treatment for these

individuals. WIP1 small molecule inhibitors have recently been developed as potential cancer therapeutic drugs (Yamaguchi *et al.*, 2006; Belova *et al.*, 2005; Rayter *et al.*, 2008), so it is possible such drugs might alleviate some A-T patient symptoms.

As described here, removal of Wip1 from *Atm* null mice partially rescued a number of Atm deficiency phenotypes. The most dramatic rescue was the reduction in thymic lymphoma incidence in double knockout mice compared to their Atm null counterparts. The mechanisms by which the absence of Wip1 reduced thymic lymphomas are likely to be related to enhanced DNA damage responses observed in the thymic tissues of the double knockout mice compared to *Atm* null mice (Fig. 2A). The ATM/ATR-initiated DNA damage response has been shown to be an important failsafe mechanism that prevents progression of precancerous lesions (Bartkova *et al.*, 2005; Halazonetis *et al.*, 2008). In particular, H2AX and p53 showed increased phosphorylation in IR-treated double null mice compared to *Atm* null mice. The increased phosphorylation of H2AX may be associated with more efficient DNA double strand break repair, consistent with our finding that reduction of Wip1 enhances this type of repair (Moon *et al.*, 2010). In addition, the p53 response was elevated in IR-treated double knockout mice compared to *Atm* null mice as measured by p53 protein levels, p53 serine 18 phosphorylation, and induction of the $p21^{Waf1/Cip1}$ gene. This increased p53 activity in the double null mice is likely a key component of their resistance to thymic lymphomas relative to *Atm* null mice.

Enhanced DNA damage responses and reduced lymphomagenesis in the double knockout mice is consistent with the reduced chromosomal instability observed in their splenocytes. ATM deficiency has been shown to be associated with increased aneuploidy and other types of chromosomal aberrations, and this has been linked to both reduced p21 and p53 expression (Shen *et al.*, 2005; Li *et al.*, 2010). The mechanisms by which absence of WIP1 promotes chromosomal stability may be multiple, beginning with augmented and prolonged phosphorylation of ATM targets involved in maintaining genomic stability. Reduction of WIP1 levels enhances the enforcement of intra-S and G2/M checkpoints (Lu *et al.*, 2005a), and an enhanced G2/M checkpoint would likely reduce aneuploidy.

Atm null mice structural disorganization in both testes and ovaries (Xu *et al.*, 1996). This phenocopies A-T patients, who also exhibit gonadal abnormalities, such as ovaries without follicle development in females and histological abnormalities and reduced spermatogenesis in males (Sedgwick and Boder, 1991). We have shown that *Wip1* null mice had modestly reduced male fertility and reduced spermatogenesis as well as moderate disorganization of seminiferous tubules (Choi *et al.*, 2002). Thus, it was surprising that absence of Wip1 was able to rescue both testicular and ovarian gametogenesis to some extent in the double knockout mice. However, the rescue of gametogenesis was variably penetrant in the double knockout mice and the reasons for this remain unclear. Wip1 is highly expressed in the testes with its highest level of expression correlating with the final stages of meiosis, suggesting that Wip1 plays a role in regulating meiosis I and II divisions to inhibit further cell cycles and maintain the haploid state (Choi *et al.*, 2002). The mechanism of rescue in the double knockout mice may involve restoration of near normal phosphorylation to meiotic proteins targeted by both Atm and Wip1.

Atm null mice and A-T patients exhibit a profound hypersensitivity to ionizing radiation (Abraham, 2001; Lavin, 2008). Not only did absence of Wip1 not rescue this particular phenotype, but it accentuated it in double knockout mice. When we examined the radiation-sensitive intestinal villi, double knockout villi showed higher levels of degeneration and disorganization, suggesting higher levels of cell death. However, examination of apoptosis markers in thymus, spleen, and intestine did not reveal increased apoptosis levels in the double knockout tissues (Fig. S3 and data not shown), as might be expected from other contexts (Demidov *et al.*, 2007; Xia *et al.*, 2009). Instead, non-apoptotic mechanisms of cell death may be responsible. Nevertheless, the increased hypersensitivity of double knockout mice suggest a possible synthetic lethality between *Atm* and *Wip1* deficiency, reminiscent of synthetic lethalities between Atm and other molecules (Gurley and Kemp, 2001; Jiang *et al.*, 2009; Williamson *et al.*, 2010).

In summary, we have shown that removing Wip1 from an *Atm* null mouse background reduced tumorigenesis, enhanced longevity, augmented the DNA damage response, decreased genomic instability, and partially rescued gametogenesis. Combined with studies showing that *Wip1* null mice are resistant to both spontaneous and oncogene-induced tumors (Nannenga *et al.*, 2006; Bulavin *et al.*, 2004), it is increasingly evident that reducing Wip1 levels can diminish cancer susceptibility. Thus, the development of Wip1 inhibitors may be beneficial in cancer treatment. Moreover, the results described here suggest that application of Wip1 inhibitors to A-T patients may be efficacious both in a preventative and therapeutic context.

Materials and Methods

Mice

$Atm^{+/-}$ mice (Borghesani *et al.*, 2000) were crossed with $Wip1^{+/-}$ mice (Choi *et al.*, 2002) to obtain $Atm^{+/-}Wip1^{+/-}$ F1 offspring. *Wip1*-deficient mice were of mixed C57BL/6 × 129/Sv background, but all mice were backcrossed at least three generations into C57BL/6. The double heterozygotes were then crossed to obtain F2 offspring of all possible *Atm/Wip1* genotypes. Genotyping of mice for *Atm* and *Wip1* mutant alleles was performed by tail DNA PCR (Moon *et al.*, 2010). Mice were allowed to age naturally and monitored for tumor formation throughout their lifespan. All tumors identified were harvested and fixed in 10% neutral buffered formalin. Severely moribund mice were sacrificed and all major organs analyzed by visual examination and histopathology. The SPSS 14.0 program was used to construct Kaplan-Meier tumor free survival plots. All animals were handled in strict accordance with good animal practice as defined by the Institutional Animal Care and Use Committee for Baylor College of Medicine and Affiliates.

Histopathological analysis of tissues and tumors

Thymic lymphomas, thymi, spleens, testes, ovaries, and small intestines were collected and placed in 10% buffered formalin. Fixed tissues were embedded in paraffin blocks, sectioned, and hematoxylin and eosin staining was performed using standard methods. Sections were examined and images were obtained with an Olympus BX50 microscope, an Olympus 40x and 200x objective, and an Olympus DP11 camera.

Western blot analysis of DNA damage response proteins in mouse lymphoid tissues

Atm$^{+/+}$*Wip1*$^{+/+}$, *Atm*$^{+/+}$*Wip1*$^{-/-}$, *Atm*$^{-/-}$*Wip1*$^{+/+}$, and *Atm*$^{-/-}$*Wip1*$^{-/-}$ eight week old male and female mice were treated with 5 Gy whole body irradiation with a ^{137}Cs source (MDS Nordion GammaCell Exactor). Six hours after IR, spleen and thymus tissues were harvested, homogenized, and lysed as previously described (Nannenga *et al.*, 2006). Lysates (20 μg) were mixed with 2× Laemmli sample buffer, boiled and loaded on 10% polyacrylamide gels. Proteins were transferred to PVDF membrane and detected using the indicated primary antibody to the protein or protein phosphorylation site along with an appropriate secondary antibody. Anti-p53(p15S) (cat#9284), anti-p53 (cat#2524), and anti-H2AX (cat#2595) antibodies were purchased from Cell Signaling Technology. Anti-γ-H2AX (catalog #07-164) was purchased from Millipore. Anti-GAPDH protein antibody was purchased from Santa Cruz Biotechnology (cat#sc-25778). Anti-p53(p15S), anti-H2AX, anti-γ-H2AX, and anti-GAPDH antibodies were all used at 1:1000 dilution. Anti-p53 antibody was used at 1:500 dilution.

Real-time PCR

Atm$^{+/+}$*Wip1*$^{+/+}$, *Atm*$^{+/+}$*Wip1*$^{-/-}$, *Atm*$^{-/-}$*Wip1*$^{+/+}$, and *Atm*$^{-/-}$*Wip1*$^{-/-}$ eight week old male and female mice were treated with 5 Gy whole body γ-irradiation as described above. Six hours after γ-irradiation, thymi were harvested and total mRNA was extracted using TRIZOL (Invitrogen). cDNA was then synthesized using the High-Capacity cDNA Reverse Transcription Kit (Applied Biosystems) and real-time PCR was performed with RT-300 equipment (Corbett Research) with iQ SYBR Green Super Mix (Bio-Rad) using gene-specific primers for mouse p21 and β-actin. The primer sequences used were: p21F: CCATGAGCGCATCGCAATC, p21R: CCTGGTGATGTCCGACCTG, β-actinF: GACCTCTATGCCAACACAGT, β-actinR: AGTACTTGCGCTCAGGAGGA. Real-time PCR was done in duplicate for each sample, and p21 expression was normalized to β-actin levels.

Spectral karyotyping of mouse thymic lymphocytes

Spleens from *Atm*$^{+/+}$*Wip1*$^{+/+}$, *Atm*$^{+/+}$*Wip1*$^{-/-}$, *Atm*$^{-/-}$*Wip1*$^{+/+}$, and *Atm*$^{-/-}$*Wip1*$^{-/-}$ eight week old male and female mice were harvested and single cell suspensions were made in RPMI media containing 10% FBS. Cells were plated at 4 million cells/ml on 60 mm dishes with 5 μg/ml of Concanavalin A. After 72 hours, the cells were split and plated at 0.5 million cells/ml on 60 mm dishes with 100 IU/ml of IL-2 and 50% Concanavalin A conditioned media. 24 hours later the cells were prepared for spectral karyotyping (SKY) as previously described (Rao *et al.*, 1998). For SKY, the cocktail of mouse chromosome paints was obtained from Applied Spectral Imaging (ASI, Vista, CA). Hybridization and detection were carried out according to manufacturer protocol, with slight modifications. Chromosomes were counterstained with DAPI. For each mouse, 12-20 metaphases were analyzed by SKY. Images were acquired with a SD300H Spectra cube (ASI) mounted on a Zeiss Axioplan II microscope using a custom designed optical filter (SKY-1) (Chroma Technology, Brattleboro, VT), and analyzed using SKY View 2.1.1 software (ASI, Vista, CA).

Rota-rod treadmill test

Atm$^{+/+}$*Wip1*$^{+/+}$, *Atm*$^{+/+}$*Wip1*$^{-/-}$, *Atm*$^{-/-}$*Wip1*$^{+/+}$, and *Atm*$^{-/-}$*Wip1*$^{-/-}$ eight week old littermate male and female mice were tested for motor coordination using a rotating rod (UGO BASILE) in which the speed increases linearly over time as previously described (Moretti *et al.*, 2005). Mice were placed on the rota-rod that accelerates from 4-40 rpm for a maximum of 5 minutes. Four trials/day/mouse were performed for 3 consecutive days with an inter-trial interval of 30 minutes. Mice were monitored during the trial for loss of control, where the mouse holds onto the rod without walking on top or falling off, and this time was recorded.

Flow cytometric analysis of lymphocytes

Cells were prepared from thymi and spleens of *Atm*$^{+/+}$*Wip1*$^{+/+}$, *Atm*$^{+/+}$*Wip1*$^{-/-}$, *Atm*$^{-/-}$*Wip1*$^{+/+}$, and *Atm*$^{-/-}$*Wip1*$^{-/-}$ eight week old male and female mice, stained with fluorescent antibodies, fixed with 0.1% paraformaldehyde (PFA)/PBS solution, and data was collected using a CantoII flow cytometer. Thymocytes were incubated with antibodies for PE-Cy5 anti-mouse CD3e (cat#15-0031-81), FITC anti-mouse CD4 (cat#11-0041-82), and PE anti-mouse CD8a (cat#12-0081-81) from eBioscience. All antibodies were used at 4 μg/ml concentrations.

Statistical analysis

The results shown are means ± standard error. Statistical significance for most assays was assessed using the Student's *t*-test. Statistical significance for survival curves was assessed by Kaplan-Meier analyses.

Supplementary Material

Refer to Web version on PubMed Central for supplementary material.

Acknowledgments

We thank Corrine Spencer and Yi-Jue Zhao for technical assistance. This work was supported by NIH grants (R01 CA100420) to L.A.D. and (R01 CA136549) to X.L., and a DOD Breast Cancer Research Program Predoctoral Traineeship Award (BC050781) to T.-A.N.

References

Abraham RT. Cell cycle checkpoint signaling through the ATM and ATR kinases. Genes Dev. 2001; 15:2177–2196. [PubMed: 11544175]

Appella E, Anderson CW. Post-translational modifications and activation of p53 by genotoxic stresses. European J Biochem. 2001; 268:2764–2772. [PubMed: 11358490]

Barlow C, Hirotsune S, Paylor R, Liyanage M, Eckhaus M, Collins F, et al. Atm-deficient mice: a paradigm of ataxia telangiectasia. Cell. 1996; 86:159–171. [PubMed: 8689683]

Bartkova J, Horejsi Z, Koed K, Kramer A, Tort F, Zieger K, et al. DNA damage response as a candidate anti-cancer barrier in early human tumorigenesis. Nature. 2005; 434:864–870. [PubMed: 15829956]

Belova GI, Demidov ON, Fornace AJ, Bulavin DV. Chemical inhibition of Wip1 phosphatase contributes to suppression of tumorigenesis. Cancer Biol Ther. 2005; 4:1154–1158. [PubMed: 16258255]

Borghesani PR, Alt FW, Bottaro A, Davidson L, Aksoy S, Rathbun GA, et al. Abnormal development of Purkinje cells and lymphocytes in Atm mutant mice. Proc Natl Acad Sci USA. 2000; 97:3336–3341. [PubMed: 10716718]

Bulavin DV, Demidov ON, Saito S, Kauraniemi P, Phillips C, Amundson SA, et al. Amplification of PPM1D in human tumors abrogates p53 tumor-suppressor activity. Nat Genet. 2002; 31:210–215. [PubMed: 12021785]

Bulavin DV, Phillips C, Nannenga B, Timofeev O, Donehower LA, Anderson CW, et al. Inactivation of the Wip1 phosphatase inhibits mammary tumorigenesis through p38 MAPK-mediated activation of the p16(Ink4a)-p19(Arf) pathway. Nat Genet. 2004; 36:343–350. [PubMed: 14991053]

Castellino RC, De Bortoli M, Lu X, Moon SH, Nguyen TA, Shepard MA, et al. Medulloblastomas overexpress the p53-inactivating oncogene WIP1/PPM1D. J Neurooncol. 2008; 86:245–256. [PubMed: 17932621]

Choi J, Nannenga B, Demidov ON, Bulavin DV, Cooney A, Brayton C, et al. Mice deficient for the wild-type p53-induced phosphatase gene (Wip1) exhibit defects in reproductive organs, immune function, and cell cycle control. Mol Cell Biol. 2002; 22:1094–1105. [PubMed: 11809801]

Chun HH, Gatti RA. Ataxia-telangiectasia, an evolving phenotype. DNA Repair (Amst.). 2004; 3:1187–1196. [PubMed: 15279807]

Demidov ON, Timofeev O, Lwin HN, Kek C, Appella E, Bulavin DV. Wip1 phosphatase regulates p53-dependent apoptosis of stem cells and tumorigenesis in the mouse intestine. Cell Stem Cell. 2007; 1:180–190. [PubMed: 18371349]

Ehrbrecht A, Muller U, Wolter M, Hoischen A, Koch A, Radlwimmer B, et al. Comprehensive genomic analysis of desmoplastic medulloblastomas: identification of novel amplified genes and separate evaluation of the different histological components. J Pathol. 2006; 208:554–563. [PubMed: 16400626]

El-Deiry WS, Tokino T, Velculescu VE, Levy DB, Parsons R, Trent JM, et al. WAF1, a potential mediator of p53 tumor suppression. Cell. 1993; 19:817–825. [PubMed: 8242752]

Elson A, Wang Y, Daugherty CJ, Morton CC, Zhou F, Campos-Torres J, et al. Pleiotropic defects in ataxia-telangiectasia protein-deficient mice. Proc Natl Acad Sci USA. 1996; 93:13084–13089. [PubMed: 8917548]

Fiscella M, Zhang HL, Fan SJ, Sakaguchi K, Shen SF, Mercer WE, et al. Wip1, a novel human protein phosphatase that is induced in response to ionizing radiation in a p53-dependent manner. Proc Natl Acad Sci USA. 1997; 94:6048–6053. [PubMed: 9177166]

Fujimoto H, Onishi N, Kato N, Takekawa M, Xu X, Kosugi A, et al. Regulation of the antioncogenic Chk2 kinase by the oncogenic Wip1 phosphatase. Cell Death Different. 2006; 13:1170–1180.

Gurley KE, Kemp CJ. Synthetic lethality between mutation in Atm and DNA-PK(cs) during murine embryogenesis. Curr Biol. 2001; 11:191–194. [PubMed: 11231155]

Halazonetis TD, Gorgoulis VG, Bartek J. An oncogene-induced DNA damage model for cancer development. Science. 2008; 319:1352–1355. [PubMed: 18323444]

Harrison M, Li J, Degenhardt Y, Hoey T, Powers S. Wip1-deficient mice are resistant to common cancer genes. Trends Mol Med. 2004; 10:359–361. [PubMed: 15310454]

Herzog KH, Chong MJ, Kapsetaki M, Morgan JI, McKinnon PJ. Requirement for Atm in ionizing radiation-induced cell death in the developing central nervous system. Science. 1998; 280:1089–1091. [PubMed: 9582124]

Hirasawa A, Saito-Ohara F, Inoue J, Aoki D, Susumu N, Yokoyama T, et al. Association of 17q21-q24 gain in ovarian clear cell adenocarcinomas with poor prognosis and identification of PPM1D and APPBP2 as likely amplification targets. Clin Cancer Res. 2003; 9:1995–2004. [PubMed: 12796361]

Ito K, Hirao A, Arai F, Matsuoka S, Takubo K, Hamaguchi I, et al. Regulation of oxidative stress by ATM is required for self-renewal of haematopoietic stem cells. Nature. 2004; 431:997–1002. [PubMed: 15496926]

Jiang H, Reinhardt HC, Bartkova J, Tommiska J, Blomqvist C, Nevanlinna H, et al. The combined status of ATM and p53 link tumor development with therapeutic response. Genes Dev. 2009; 23:1895–1909. [PubMed: 19608766]

Lavin MF. ATM and the Mre11 complex combine to recognize and signal DNA double-strand breaks. Oncogene. 2007; 26:7749–7758. [PubMed: 18066087]

Lavin MF. Ataxia-telangiectasia: from a rare disorder to a paradigm for cell signalling and cancer. Nat Rev Mol Cell Biol. 2008; 9:759–769. [PubMed: 18813293]

Le Guezennec X, Bulavin DV. WIP1 phosphatase at the crossroads of cancer and aging. Trends Biochem Sci. 2009; 35:109–114. [PubMed: 19879149]

Li J, Yang Y, Peng Y, Austin RJ, van Eyndhoven G, Nguyen KCQ, et al. Oncogenic properties of PPM1D located within a breast cancer amplification epicenter at 17q23. Nat Genet. 2002; 31:133–134. [PubMed: 12021784]

Li M, Fang X, Baker DJ, Guo L, Gao X, Wei Z, et al. The ATM-p53 pathway suppresses aneuploidy-induced tumorigenesis. Proc Natl Acad Sci USA. 2010; 107:14188–14193. [PubMed: 20663956]

Loukopoulos P, Shibata T, Katoh H, Kokubu A, Sakamoto M, Yamazaki K, et al. Genome-wide array-based comparative genomic hybridization analysis of pancreatic adenocarcinoma: Identification of genetic indicators that predict patient outcome. Cancer Sci. 2007; 98:392–400. [PubMed: 17233815]

Lu X, Ma O, Nguyen TA, Jones SN, Oren M, Donehower LA. The Wip1 Phosphatase acts as a gatekeeper in the p53-Mdm2 autoregulatory loop. Cancer Cell. 2007; 12:342–354. [PubMed: 17936559]

Lu X, Nannenga B, Donehower LA. PPM1D dephosphorylates Chk1 and p53 and abrogates cell cycle checkpoints. Genes Dev. 2005a; 19:1162–1174. [PubMed: 15870257]

Lu XB, Nguyen TA, Donehower LA. Reversal of the ATM/ATR-mediated DNA damage response by the oncogenic phosphatase PPM1D. Cell Cycle. 2005b; 4:1060–1064. [PubMed: 15970689]

Lu X, Nguyen TA, Moon SH, Darlington Y, Sommer M, Donehower LA. The type 2C phosphatase Wip1: an oncogenic regulator of tumor suppressor and DNA damage response pathways. Cancer Metastasis Rev. 2008; 27:123–135. [PubMed: 18265945]

Macurek L, Lindqvist A, Voets O, Kool J, Vos HR, Medema RH. Wip1 phosphatase is associated with chromatin and dephosphorylates gammaH2AX to promote checkpoint inhibition. Oncogene. 2010; 29:2281–2291. [PubMed: 20101220]

Moon SH, Lin L, Zhang X, Nguyen TA, Darlington Y, Waldman AS, et al. Wildtype p53-induced phosphatase 1 dephosphorylates histone variant {gamma}-H2AX and suppresses DNA double strand break repair. J Biol Chem. 2010; 285:12935–12947. [PubMed: 20118229]

Moretti P, Bouwknecht JA, Teague R, Paylor R, Zoghbi HY. Abnormalities of social interactions and home-cage behavior in a mouse model of Rett syndrome. Hum Mol Genet. 2005; 14:205–220. [PubMed: 15548546]

Nannenga B, Lu X, Dumble M, Van Maanen M, Nguyen TA, Sutton R, et al. Augmented cancer resistance and DNA damage response phenotypes in PPM1D null mice. Mol Carcinog. 2006; 45:594–604. [PubMed: 16652371]

Rao PH, Cigudosa JC, Ning Y, Calasanz MJ, Iida S, Tagawa S, et al. Multicolor spectral karyotyping identifies new recurring breakpoints and translocations in multiple myeloma. Blood. 1998; 92:1743–1748. [PubMed: 9716604]

Rayter S, Elliott R, Travers J, Rowlands MG, Richardson TB, Boxall K, et al. A chemical inhibitor of PPM1D that selectively kills cells overexpressing PPM1D. Oncogene. 2008; 27:1036–1044. [PubMed: 17700519]

Rotman G, Shiloh Y. ATM: from gene to function. Hum Mol Genet. 1998; 7:1555–1563. [PubMed: 9735376]

Saito-Ohara F, Imoto I, Inoue J, Hosoi H, Nakagawara A, Sugimoto T, et al. PPM1D is a potential target for 17q gain in neuroblastoma. Cancer Res. 2003; 63:1876–1883. [PubMed: 12702577]

Savitsky K, Sfez S, Tagle DA, Ziv Y, Sartiel A, Collins FS, et al. The complete sequence of the coding region of the ATM gene reveals similarity to cell cycle regulators in different species. Hum Mol Genet. 1995; 4:2025–2032. [PubMed: 8589678]

Schito ML, Demidov ON, Saito S, Ashwell JD, Appella E. Wip1 phosphatase-deficient mice exhibit defective T cell maturation due to sustained p53 activation. J Immunol. 2006; 176:4818–4825. [PubMed: 16585576]

Sedgwick, RP.; Boder, E.; Ataxia-Telangiectasia. Hereditary Neuropathies and Spinocerebellar Atrophies. deJong, JMBE., editor. Elsevier; New York: 1991. p. 347-423.Vinken PJ, Bruyn GW, Klawans HL, eds. Handbook of Clinical Neurology, vol 16

Shen KC, Heng H, Wang Y, Lu S, Liu G, Deng CX, et al. ATM and p21 cooperate to suppress aneuploidy and subsequent tumor development. Cancer Res. 2005; 65:8747–8753. [PubMed: 16204044]

Shiloh Y. ATM and related protein kinases: safeguarding genome integrity. Nat Rev Cancer. 2003; 3:155–168. [PubMed: 12612651]

Shreeram S, Demidov ON, Hee WK, Yamaguchi H, Onishi N, Kek C, et al. Wip1 phosphatase modulates ATM-dependent signaling pathways. Mol Cell. 2006a; 23:757–764. [PubMed: 16949371]

Shreeram S, Hee WK, Demidov ON, Kek C, Yamaguchi H, Fornace AJ, et al. Regulation of ATM/p53-dependent suppression of myc-induced lymphomas by Wip1 phosphatase. J Exp Med. 2006b; 203:2793–2799. [PubMed: 17158963]

Takekawa M, Adachi M, Nakahata A, Nakayama I, Itoh F, et al. p53-inducible Wip1 phosphatase mediates a negative feedback regulation of p38 MAPK-p53 signaling in response to UV radiation. EMBO J. 2000; 19:6517–6526. [PubMed: 11101524]

Tan DS, Lambros MB, Rayter S, Natrajan R, Vatcheva R, Gao Q, et al. PPM1D is a potential therapeutic target in ovarian clear cell carcinomas. Clin Cancer Res. 2009; 15:2269–2280. [PubMed: 19293255]

Westphal CH, Rowan S, Schmaltz C, Elson A, Fisher DE, Leder P. Atm and p53 cooperate in apoptosis and suppression of tumorigenesis, but not in resistance to acute radiation toxicity. Nat Genet. 1997; 16:397–401. [PubMed: 9241281]

Williamson CT, Muzik H, Turhan AG, Zamo A, O'Connor MJ, Bebb DG, et al. ATM deficiency sensitizes mantle cell lymphoma cells to poly(ADP-ribose) polymerase-1 inhibitors. Mol Cancer Ther. 2010; 9:347–357. [PubMed: 20124459]

Xia Y, Ongusaha P, Lee SW, Liou YC. Loss of Wip1 sensitizes cells to stress- and DNA damage-induced apoptosis. J Biol Chem. 2009; 284:17428–17437. [PubMed: 19395378]

Xu Y, Ashley T, Brainerd EE, Bronson RT, Meyn MS, Baltimore D. Targeted disruption of ATM leads to growth retardation, chromosomal fragmentation during meiosis, immune defects, and thymic lymphoma. Genes Dev. 1996; 10:2411–2422. [PubMed: 8843194]

Yamaguchi H, Durell SR, Feng HQ, Bai YW, Anderson CW, Appella E. Development of a substrate-based cyclic phosphopeptide inhibitor of protein phosphatase 2C delta, Wip1. Biochemistry. 2006; 45:13193–13202. [PubMed: 17073441]

Yoda A, Toyoshima K, Watanabe Y, Onishi N, Hazaka Y, Tsukuda Y, et al. Arsenic trioxide augments Chk2/p53-mediated apoptosis by inhibiting oncogenic Wip1 phosphatase. J Biol Chem. 2008; 283:18969–18979. [PubMed: 18482988]

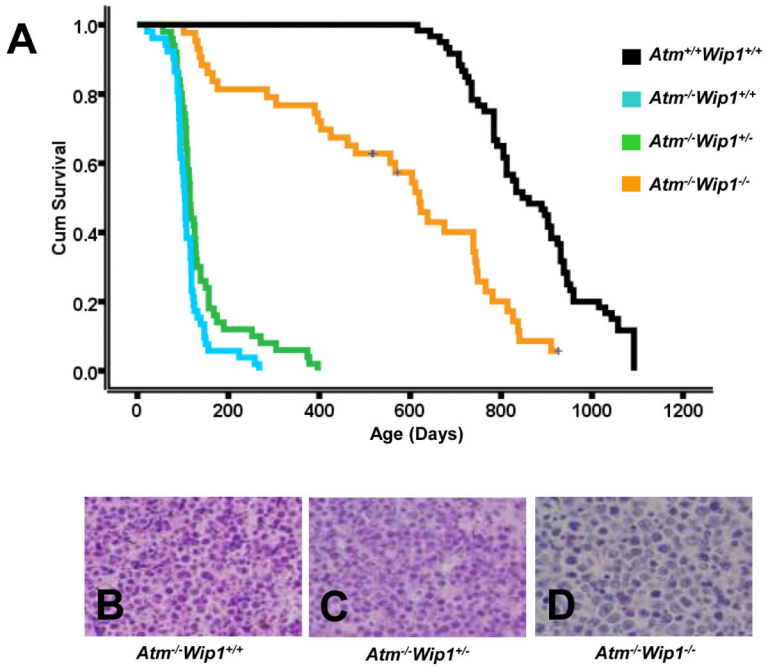

Figure 1. *Atm*$^{-/-}$*Wip1*$^{-/-}$ mice exhibit extended survival and protection from thymic lymphomas

(A) Kaplan-Meier survival plot comparing *Atm*$^{+/+}$*Wip1*$^{+/+}$ (N=55), *Atm*$^{-/-}$*Wip1*$^{+/+}$ (N=52), *Atm*$^{-/-}$*Wip1*$^{+/-}$ (N=50), and *Atm*$^{-/-}$*Wip1*$^{-/-}$ (N=43) mouse longevity. *Atm*$^{-/-}$*Wip1*$^{-/-}$ mice are largely protected from developing thymic lymphomas and survive much longer than their *Atm*$^{-/-}$*Wip1*$^{+/+}$ and *Atm*$^{-/-}$*Wip1*$^{+/-}$ counterparts ($P = 2.42 \times 10^{-14}$). (B-D) Representative hematoxylin and eosin stained sections of thymic lymphomas at 200X magnification from *Atm*$^{-/-}$*Wip1*$^{+/+}$ (B), *Atm*$^{-/-}$*Wip1*$^{+/-}$ (C), and *Atm*$^{-/-}$*Wip1*$^{-/-}$ (D) mice. No differences in histopathology were observed in the thymic lymphomas from *Atm*$^{-/-}$*Wip1*$^{-/-}$ (N=3) mice when compared to *Atm*$^{-/-}$*Wip1*$^{+/+}$ (N=3) and *Atm*$^{-/-}$*Wip1*$^{+/-}$ (N=3) littermates.

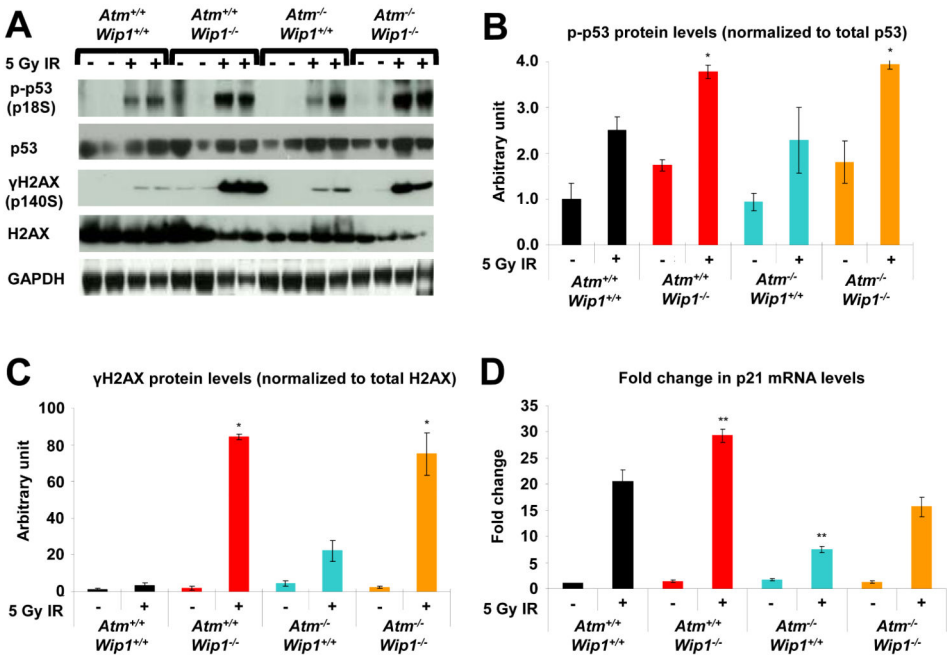

Figure 2. Absence of Wip1 enhances p53 and DNA damage responses in *Atm* null mice

(A) DNA damage-induced phosphorylation of p53 and H2AX is enhanced in thymic tissues of mice lacking Wip1. $Atm^{+/+}Wip1^{+/+}$, $Atm^{-/-}Wip1^{+/+}$, $Atm^{+/+}Wip1^{-/-}$, and $Atm^{-/-}Wip1^{-/-}$ mice were treated with 5 Gy of IR. Six hours after radiation, thymus tissue was harvested from each mouse. Protein lysates from individual mouse thymi were subjected to Western blot analysis with antibodies specific for the indicated proteins or their phosphorylated forms. (B) Quantitation of p53 phosphorylation at serine 18 in thymus lysates from untreated and IR-treated $Atm^{+/+}Wip1^{+/+}$, $Atm^{-/-}Wip1^{+/+}$, $Atm^{+/+}Wip1^{-/-}$, and $Atm^{-/-}Wip1^{-/-}$ mice. (C) Quantitation of H2AX phosphorylation (γ-H2AX) at serine 140 in thymus lysates from untreated and IR-treated $Atm^{+/+}Wip1^{+/+}$, $Atm^{-/-}Wip1^{+/+}$, $Atm^{+/+}Wip1^{-/-}$, and $Atm^{-/-}Wip1^{-/-}$ mice. (D) Quantitation of of p21 RNA expression in unirradiated and irradiated $Atm^{+/+}Wip1^{+/+}$, $Atm^{-/-}Wip1^{+/+}$, $Atm^{+/+}Wip1^{-/-}$, and $Atm^{-/-}Wip1^{-/-}$ mouse thymi by real-time PCR. For each of the genotype/radiation cohorts, results were calculated from four different animals and averaged for the graphs. Only two animals for each genotype radiation cohort are shown in Figure 2A, however. Asterisks (**P<0.01, *P<0.05) indicate significant differences in the magnitude of IR-induced increases compared to IR-induced increases in the wildtype mice.

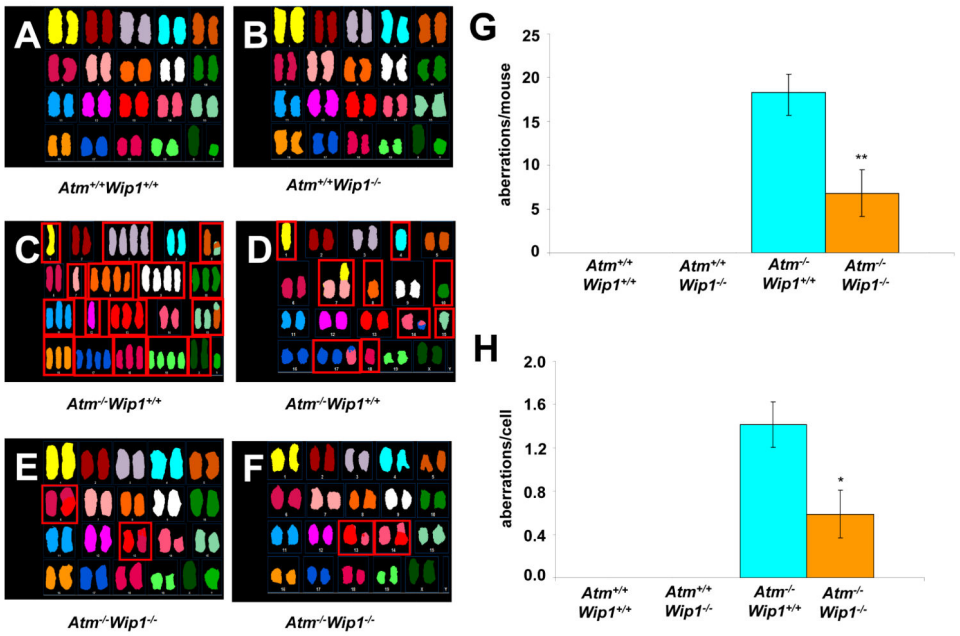

Figure 3. Absence of Wip1 increases genomic stability of *Atm* null splenocytes

(A-F) SKY analysis of $Atm^{+/+}Wip1^{+/+}$ (N=4) (A), $Atm^{+/+}Wip1^{-/-}$ (N=4) (B), $Atm^{-/-}Wip1^{+/+}$ (N=6) (C,D), and $Atm^{-/-}Wip1^{-/-}$ (N=5) (E,F) splenocytes. Aberrant chromosomes (either non-diploid numbers or translocations) are indicated by red boxes. $Atm^{-/-}Wip1^{-/-}$ splenocytes have decreased genomic instability compared to $Atm^{-/-}Wip1^{+/+}$ splenocytes. (G) Graph comparing the average number of chromosomal aberrations observed per mouse (12-20 metaphase profiles analyzed per mouse and normalized) using SKY analysis. $Atm^{-/-}Wip1^{-/-}$ splenocytes have a decreased number of chromosomal aberrations per mouse compared to $Atm^{-/-}Wip1^{+/+}$ splenocytes. $^{**}P = 0.009$. (H) Graph comparing the average number of chromosomal aberrations per cell for each genotype. $Atm^{-/-}Wip1^{-/-}$ splenocytes have a reduced number of chromosomal aberrations per cell observed compared to $Atm^{-/-}Wip1^{+/+}$ splenocytes. $^{*}P = 0.03$.

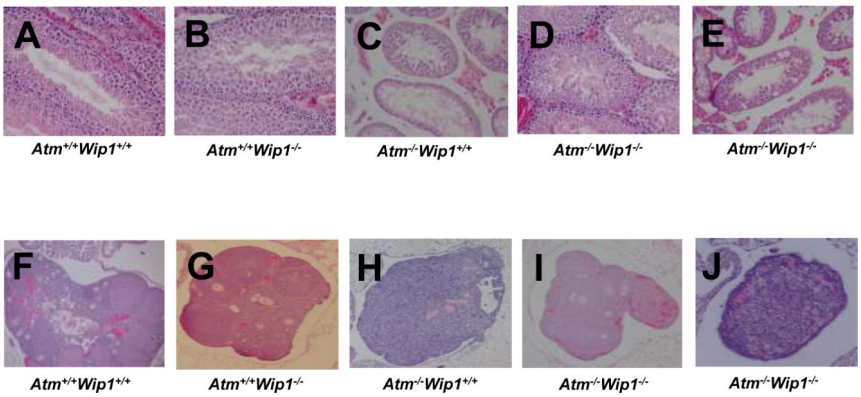

Figure 4. *Atm*$^{-/-}$*Wip1*$^{-/-}$ mice exhibit partial restoration of mature gamete formation

(A-E) Representative hematoxylin and eosin (H&E) stained sections of testes from *Atm*$^{+/+}$*Wip1*$^{+/+}$ (N=4) (A), *Atm*$^{+/+}$*Wip1*$^{-/-}$ (N=4) (B), *Atm*$^{-/-}$*Wip1*$^{+/+}$ (N=6) (C), and *Atm*$^{-/-}$*Wip1*$^{-/-}$ (N=9) (D & E) mice at 200X magnification. Some testes from *Atm*$^{-/-}$*Wip1*$^{-/-}$ mice show a partial rescue of spermatogenesis similar to that observed in testes from *Atm*$^{+/+}$*Wip1*$^{-/-}$ mice. (F-J) H&E stained sections of ovaries from *Atm*$^{+/+}$*Wip1*$^{+/+}$ (N=4) (F), *Atm*$^{+/+}$*Wip1*$^{-/-}$ (N=5) (G), *Atm*$^{-/-}$*Wip1*$^{+/+}$ (N=4) (H), and *Atm*$^{-/-}$*Wip1*$^{-/-}$ (N=3) (I & J) mice at 40X magnification. Some *Atm*$^{-/-}$*Wip1*$^{-/-}$ ovaries show a partial rescue of oogenesis similar to that observed in *Atm*$^{+/+}$*Wip1*$^{-/-}$ ovaries.

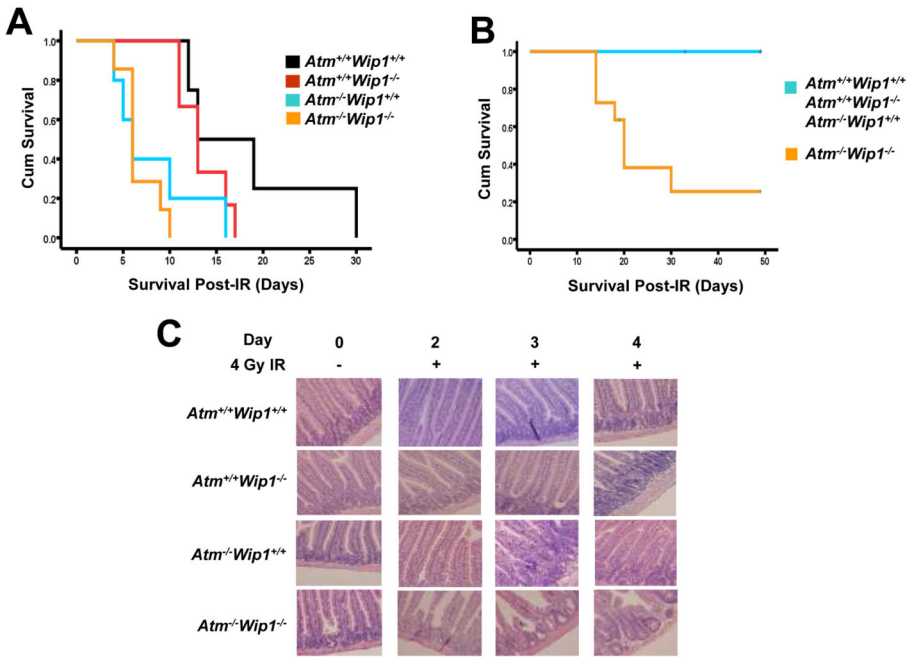

Figure 5. *Atm*$^{-/-}$*Wip1*$^{-/-}$ mice are more sensitive to IR than *Atm*$^{-/-}$*Wip1*$^{+/+}$ mice

(A) Survival plot comparing survival of *Atm*$^{+/+}$*Wip1*$^{+/+}$ (N=4), *Atm*$^{+/+}$*Wip1*$^{-/-}$ (N=6), *Atm*$^{-/-}$*Wip1*$^{+/+}$ (N=5), and *Atm*$^{-/-}$*Wip1*$^{-/-}$ (N=7) mice after whole body IR with 8 Gy. *Atm*$^{-/-}$*Wip1*$^{+/+}$ and *Atm*$^{-/-}$*Wip1*$^{-/-}$ mice are more sensitive to IR compared to *Atm*$^{+/+}$*Wip1*$^{+/+}$ mice. This difference approached significance ($P = 0.06$). (B) Survival plot comparing survival of *Atm*$^{+/+}$*Wip1*$^{+/+}$ (N=5), *Atm*$^{+/+}$*Wip1*$^{-/-}$ (N=6), *Atm*$^{-/-}$*Wip1*$^{+/+}$ (N=10), and *Atm*$^{-/-}$*Wip1*$^{-/-}$ (N=11) mice after whole body IR with 4 Gy. *Atm*$^{-/-}$*Wip1*$^{-/-}$ mice are significantly more sensitive to IR compared to their *Atm*$^{-/-}$*Wip1*$^{+/+}$ counterparts ($P = 0.002$). (C) Representative H&E stained sections of small intestines of *Atm*$^{+/+}$*Wip1*$^{+/+}$ (N=3), *Atm*$^{+/+}$*Wip1*$^{-/-}$ (N=3), *Atm*$^{-/-}$*Wip1*$^{+/+}$ (N=3), and *Atm*$^{-/-}$*Wip1*$^{-/-}$ (N=3) mice after whole body IR with 4 Gy or unirradiated and collected 2, 3, and 4 days after treatment. The small intestines of the *Atm*$^{-/-}$*Wip1*$^{-/-}$ mice display an enhanced radiation toxicity phenotype compared to other genotypes.

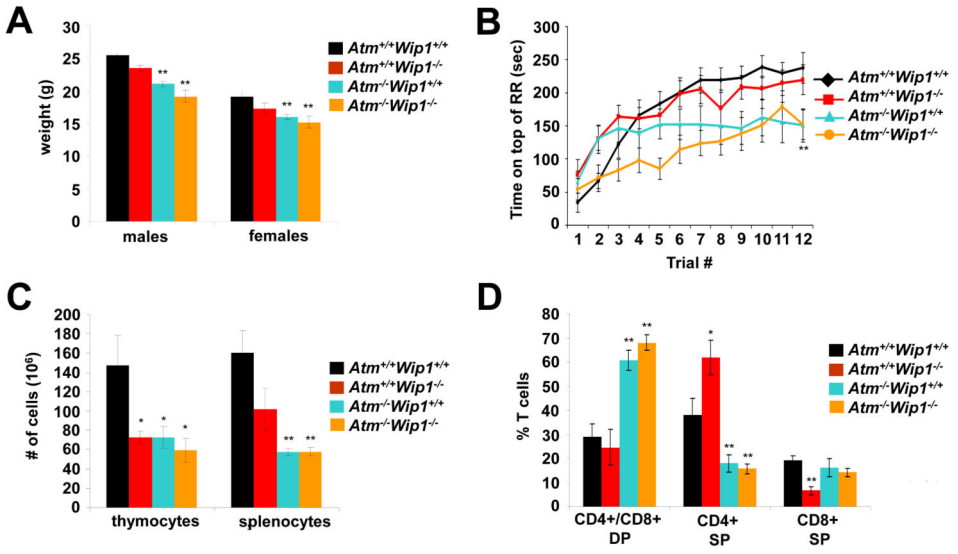

Figure 6. Absence of Wip1 does not rescue somatic growth, motor coordination defects, or immunologic abnormalities in *Atm* null mice

(A) Absence of Wip1 does not rescue somatic growth. Male and female $Atm^{+/+}Wip1^{+/+}$ (N=16 males, 8 females), $Atm^{+/+}Wip1^{-/-}$ (N=10 males, 7 females), $Atm^{-/-}Wip1^{+/+}$ (N=9 males, 13 females), and $Atm^{-/-}Wip1^{-/-}$ (N=7 males, 11 females) mice were weighed at 8 weeks of age. $Atm^{-/-}Wip1^{+/+}$ and $Atm^{-/-}Wip1^{-/-}$ males and females exhibited a significantly reduced bodyweight compared to $Atm^{+/+}Wip1^{+/+}$ mice. (B) Absence of Wip1 does not rescue motor coordination defects. Using the rota-rod treadmill test, $Atm^{-/-}Wip1^{+/+}$ (N=12) and $Atm^{-/-}Wip1^{-/-}$ (N=10) mice exhibit significant motor coordination defects compared to their $Atm^{+/+}Wip1^{+/+}$ (N=12) and $Atm^{+/+}Wip1^{-/-}$ (N=14) counterparts. (C) Absence of Wip1 does not rescue lymphoid cell depletion. Thymocytes and splenocytes were collected from $Atm^{+/+}Wip1^{+/+}$, $Atm^{+/+}Wip1^{-/-}$, $Atm^{-/-}Wip1^{+/+}$, and $Atm^{-/-}Wip1^{-/-}$ mice at 8 weeks of age, (N=10 for all genotypes) and counted. The $Atm^{-/-}Wip1^{-/-}$ mice have significantly decreased numbers of both splenocytes and thymocytes compared to $Atm^{+/+}Wip1^{+/+}$ mice but not compared to $Atm^{-/-}Wip1^{+/+}$ mice. (D) Absence of Wip1 does not rescue defective thymocyte maturation. Thymocytes were collected from $Atm^{+/+}Wip1^{+/+}$, $Atm^{+/+}Wip1^{-/-}$, $Atm^{-/-}Wip1^{+/+}$, and $Atm^{-/-}Wip1^{-/-}$ mice at 8 weeks of age, (N=10 for all genotypes). Thymocyte expression of CD3, CD4, and CD8 was examined using flow cytometry. $Atm^{-/-}Wip1^{-/-}$ thymocytes show a decrease in mature T cells similar to $Atm^{-/-}Wip1^{+/+}$ thymocytes. Also, both $Atm^{-/-}Wip1^{+/+}$ and $Atm^{-/-}Wip1^{-/-}$ thymocytes show a decrease in the CD4 single positive population compared to $Atm^{+/+}Wip1^{+/+}$. Asterisks in panels A, C, and D represent a significant difference between the indicated population and the control $Atm^{+/+}Wip1^{+/+}$ mice as measured by t test. $*P < 0.05$ and $**P < 0.01$.

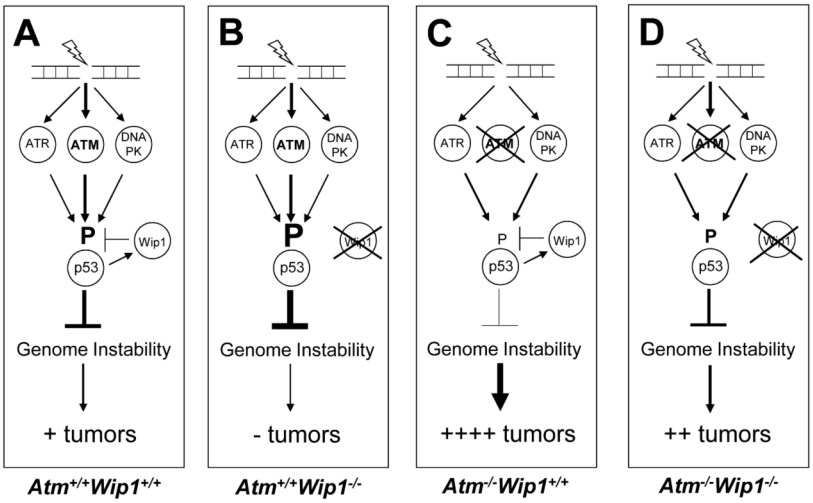

Figure 7. Model showing how Wip1 may compensate for *Atm* deficiency to partially rescue A-T-associated tumor phenotypes

(A) In $Atm^{+/+}Wip1^{+/+}$ animals, DNA damage activates Atm, which phosphorylates many targets, including p53, to activate the DNA damage response and prevent genomic instability. Normal Wip1 activity then modulates and reduces phosphorylation of p53 and other Atm targets. This overall robust DNA damage response protects against tumor formation. (B) In $Atm^{+/+}Wip1^{-/-}$ animals, phosphorylation of Atm targets is increased by absence of Wip1, resulting in an augmented DNA damage response, enhanced genomic stability, and virtually no tumors. (C) In $Atm^{-/-}Wip1^{+/+}$ animals, phosphorylation of Atm targets is decreased and only partially compensated by other PIKKs such as Atr and DNA-PK, resulting in genomic instability and a high rate of cancers. (D) In $Atm^{-/-}Wip1^{-/-}$ animals, compensatory phosphorylation of Atm targets by Atr and DNA-PK is increased and prolonged by absence of Wip1, allowing for an enhanced DNA damage response, partial restoration of genomic stability, and fewer tumors than in the $Atm^{-/-}Wip1^{+/+}$ animals.